Advances in Nano Research, *Vol. 16, No. 1 (2024) 41-52*
https://doi.org/10.12989/anr.2024.16.1.041

Rational design of rare-earth orthoferrite $LnFeO_3$ via Ln variation towards high photo-Fenton degradation of organics

Thi T. N. Phan*[1,2], Aleksandar N. Nikoloski[1a], Parisa A. Bahri[1b], Dan Li**[1]

[1]*College of Science, Technology, Engineering & Mathematics, Murdoch University, Murdoch, WA, Australia*
[2]*Department of Organic and Petrochemical Technology, School of Chemical Engineering, Hanoi University of Science and Technology, Ha Noi, Viet Nam*

(*Received March 13, 2023, Revised December 5, 2023, Accepted January 4, 2024*)

Abstract. In this study, rare-earth orthoferrites $LnFeO_3$ were synthesized using a facile hydrothermal reaction and their visible-light-induced photo-Fenton degradation of organics was optimized through Ln variation (Ln = La, Pr, or Gd). The morphological, structural, and chemical characteristics of as-prepared samples were examined in detail by using different methods, including XRD, SEM, TEM, XPS, etc. On the other side, under visible light illumination, the photo-Fenton-like catalytic activities of $LnFeO_3$ were assessed in terms of the removal of selected organic models, i.e., pharmaceuticals (ketoprofen and tetracycline) and dyes (rhodamine B and methyl orange). As compared with $PrFeO_3$ or $GdFeO_3$, the sample of $LaFeO_3$ displayed more structural distortion, larger specific surface area, and narrower band gap, resulting in its higher photo-Fenton-like catalytic activity toward the degradation of organics. In organic-containing solution, in which the initial solution pH = 5, catalyst dosage = 1 g/L and H_2O_2 concentration = 10 mM, 98.2% of rhodamine B, 31.1% of methyl orange, 67.7% of ketoprofen, or 96.4% of tetracycline was removed after 90-min exposure to simulated visible light. Our findings revealed that variation of Ln site on rare-earth orthoferrites was an effective strategy for optimizing their organic removal *via* visible-light-induced photo-Fenton reaction.
Keywords: dye; pharmaceutical; photo-Fenton; rare-earth orthoferrite

1. Introduction

In recent days, the continuous discharge of a large amount of organic-containing wastewater from various industries into natural water environment has been recognized as a public concern, possessing ecological threats and potential risks to aquatic life and human health (Soon and Hameed 2011). Dye is one of the main categories of organic pollutants, which are typically characterized by intense colour and toxicity nature (Thakur *et al*. 2022). Each year, during production and manufacturing, tens of thousands of tons of dyeing wastewater needs to be properly treated before its release to environment (Chequer *et al*. 2013). Pharmaceuticals, on the other hand, are a large group of substances that are particularly utilized for prevention, treatment, and cure of diseases in both humans and animals. There is a growing concern on the rising use and then inappropriate disposal of pharmaceuticals, causing their occurrence in wastewater, groundwater and even drinking water (Shah and Rather 2021). Conventional processes which are commonly used at many of existing wastewater treatment plants, such as adsorption, coagulation, and filtration, have been investigated to remove dyestuffs and pharmaceuticals from wastewater; but still were seen with limitations to meet stringent environmental requirements in current standards and regulations (Bansal *et al*. 2018, Martínez-Huitle and Brillas 2009). Therefore, alternative treatment techniques need to be explored and developed. Advanced oxidation processes (AOPs) have been suggested as viable and effective techniques of decomposing persistent organic pollutants from water or wastewater (Oturan and Aaron 2014). In particular, the heterogeneous photo-Fenton catalytic oxidation has been well known for its capability of complete degradation and rapid mineralization of organics (Feng *et al*. 2003, Chen *et al*. 2009, Rodríguez-Gil *et al*. 2010), thus recommended as a cost-effective, environmentally friendly, and convenient catalytic method.

Perovskite-type oxides ABO_3, which consist of rare-earth metal at A site and transition metal at B site, have emerged as a class of attractive heterogeneous catalytic materials in many of reactions, because of their high thermal stability and catalytic activity (Zhu *et al*. 2014, Deepeka *et al*. 2022). Rare-earth orthoferrites, specifically $LnFeO_3$ (Ln = rare-earth element), have been widely studied and utilized in a large range of applications, e.g., chemical sensors (Aono *et al*. 2001, Phan *et al*. 2022), catalysts (Phan *et al*. 2018a, Khalil *et al*. 2022, Khairy *et al*. 2021), and solid oxide fuel cells (Qiu *et al*. 2003). They also have shown a promising potential to act as heterogeneous photo-Fenton-like catalysts for efficient oxidation and degradation of organic pollutants under exposure to visible

*Corresponding author, Ph.D.,
E-mail: phantonga.hust@gmail.com
**Corresponding author, Ph.D.,
E-mail: l.li@murdoch.edu.au
[a] Ph.D., Professor
[b] Ph.D., Professor

ISSN: 2287-237X (Print), 2287-2388 (Online)

Table 1 Chemical structure, MW (molecular weight), empirical formula, and CAS (Chemical Abstracts Service) number for our selected organics in the study

Organic	Formula	Structure	MW (g.mol^{-1})	CAS
Ketoprofen	$C_{16}H_{14}O_3$	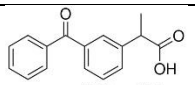	254.28	22071-15-4
Tetracycline	$C_{22}H_{24}N_2O_8$	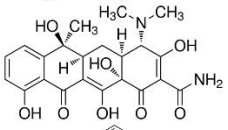	444.44	60-54-8
Rhodamine B	$C_{28}H_{31}ClN_2O_3$	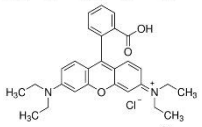	479.02	81-88-9
Methyl Orange	$C_{14}H_{14}N_3NaO_3S$	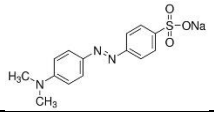	327.33	547-58-0

light (Li and Wang 2016, Li et al. 2014a, b). Khalil's group synthesized $LaFeO_3$ *via* a direct sol-gel auto-combustion method, its utilization (catalyst loading of 0.2 g/L) could achieve ~30% and ~100% removal of methylene blue (10 mg/L) in the absence and presence of 0.5 mM H_2O_2 under visible light source, respectively (Khalil *et al*. 2022). Li and wang reported that in the visible-light-assisted photo-Fenton reaction, $GdFeO_3$ nanoparticles removed 89.9% of RhB within 2 h from 30 mL of 10^{-5} mol/L RhB solution in which 30 mg $GdFeO_3$ was suspended and 1 mL of 3% H_2O_2 was added. The promising RhB photocatalytic degradation rate was over 20 times greater than that in the system of bulk $GdFeO_3$ without the addition of H_2O_2 (Li and Wang 2016). The catalytic materials, $PrFeO_3$ and $YFeO_3$, were investigated by Wang's group for their photo-Fenton-like catalytic activities over the degradation of RhB under visible light (Li *et al*. 2014b). In their study, $PrFeO_3$ showed greater visible-light-responsive catalytic performance than $YFeO_3$. After 2-h photo-Fenton reaction under the same reaction conditions (1 g/L catalyst dosage, 3% H_2O_2 and 10^{-5} mol/L RhB), $PrFeO_3$ removed 96% of RhB, whereas $YFeO_3$ only lowered 25% of RhB (Li *et al*. 2014b). Evidently, the variation on Ln site atoms in $LnFeO_3$ had a significant impact on the photo-Fenton-like catalytic activity of resulting catalytic material. However, there is little systematic investigation to understand and optimize the impact of specific Ln on the photo-Fenton-like catalytic activity of $LnFeO_3$ and then the removal of various organics, including dyes and pharmaceuticals (Xue *et al*. 2015, Ding *et al*. 2010, Niu *et al*. 2005).

In this study, as motivated by the above literature review, we prepared rare-earth orthoferrites $LnFeO_3$ using a facile hydrothermal reaction based on our previous reports (Phan *et al*. 2018a, Phan *et al*. 2018c), and optimized their visible-light-induced photo-Fenton degradation of organics through Ln variation (Ln = La, Pr, or Gd). Ketoprofen (KP) and tetracycline (TC) were selected as the models of pharmaceutical pollutants, whilst rhodamine B (RhB) and methyl orange (MO) were chosen as the models of dye pollutants. On the one side, KP, as a non-steroidal anti-inflammatory drug (NSAID), is utilized to reduce pain, swelling, or inflammation. So far, there has been no report on the removal of it *via* photo-Fenton using our selected types of $LnFeO_3$, to the best of our knowledge. TC is one of the most commonly recommeded antibiotics to treat diseases caused by various bacteria in humans and animinals (Niaei and Rostamizadeh 2020). On the other side, MO is an anionic monoazo dye and RhB is a cationic xanthene dye, both of which have been extensively used in textile, printing and photographic indutries. The above-mentioned organics have been reported with imcomplete removal at conventional wastewater treatment plant processes and attracted increasing concerns on their occurence in our ecosystems (Corcoran *et al*. 2010, Djouadi *et al*. 2018, Lee *et al*. 2013, Yesilova *et al*. 2018, Martínez *et al*. 2013, Bafana *et al*. 2011, Ahmad *et al*. 2014). Therefore, we selected KP, TC, MO and RhB as the representative pharmaceutical and dye models to investigate photo-Fenton catalytic activity of $LnFeO_3$ in this study.

2. Experimental

2.1 Material preparation

$LnFeO_3$ (Ln = La, Pr, or Gd) was synthesized *via* a hydrothermal reaction based on the literature (Phan *et al*. 2018a, c). Typically, 5 mmol $Fe(NO_3)_3.9H_2O$ (99.9%, Sigma-Aldrich) and 5 mmol $Ln(NO_3)_3.6H_2O$ (Ln = La, Pr, or Gd, 99.9%, Sigma-Aldrich) were mixed in 10 mL deionized (DI) water. After adding 10 mmol citric acid (99.9%, Sigma-Aldrich), the resulting mixture was stirred for 2 h at room temperature. Afterwards, the pH of solution was adjusted by adding NH_4OH (Biolab Ltd) to 9 and then the solution was continuously stirred for another 1 h at room temperature. The obtained solution was then heated at 180 °C for 20 h. After being cooled down, the solids were separated by centrifugation, washed with ethanol and DI water, dried at 80 °C for 5 h, and finally calcined at 800 °C for 6 h. The obtained sample, named as $LaFeO_3$, $PrFeO_3$, or $GdFeO_3$, was characterized and used in visible-light-assisted Fenton tests.

Table 2 Cell volumes, lattice constants and tolerance factors of $LaFeO_3$, $PrFeO_3$, and $GdFeO_3$

Sample	Lattice constant (Å)			Cell volume (Å^3)	Tolerance factor (t)
	a	*b*	*c*		
$LaFeO_3$	5.5566	7.8446	5.5555	242.160	0.887
$PrFeO_3$	5.4915	7.7814	5.5738	238.177	0.876
$GdFeO_3$	5.5981	7.6542	5.3424	228.916	0.849

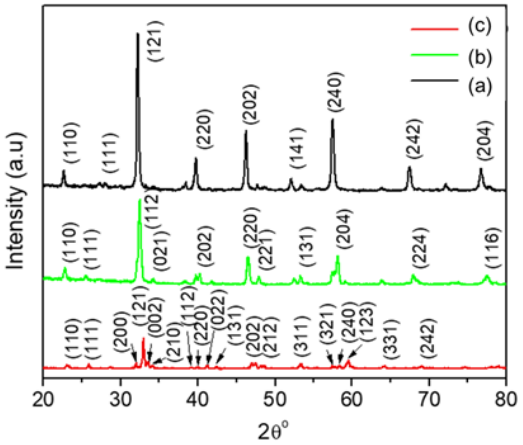

Fig. 1 XRD patterns of (a) $LaFeO_3$, (b) $PrFeO_3$, or (c) $GdFeO_3$

2.2 Material characterization

The X-ray diffraction (XRD) patterns of $LnFeO_3$ (Ln = La, Pr, and Gd) were recorded with Bruker D8 Advance diffractometer using CuKa radiation (28 mA, 35 kV). Their morphology was characterized by a scanning electron microscope (SEM) (Zeiss 1555 VP-FESEM). The nitrogen adsorption–desorption isotherm curves were measured at 77 K (SAPA2010). The chemical compositions were analyzed by an X-ray photoelectron spectroscope (XPS) (Kratos AXIS Ultra DLD). The C 1s level of carbon atom, which has a binding energy of 284.6 eV, served as the calibration standard. The UV–Vis absorption spectra were recorded with a UV–Vis spectrophotometer (Perkin Elmer Lambda 750 UV/Vis/NIR). The band gap energy was determined from the interception of a linear fitted to the low-energy side in a plot of $[F(R)h\nu]^2$ *versus* hν, in which hν is the energy of incident photon and F(R) is the Kubelka Munk function (Bellakki *et al*. 2010).

2.3 Visible light-assisted Fenton test

Typically, 100 mg $LnFeO_3$ (Ln = La, Pr, or Gd) was suspended in 100 mL solution containing organics (e.g., 10 µM KP, 10 µM TC, 10 mg/L RhB, or 10 mg/L MO, Table 1) in a cylindrical Pyrex vessel. A Xenon lamp (CEL-HX 300) with a 400 nm cut-off filter was used to provide simulated visible light on top of the solution. 10 mM H_2O_2 was added to the suspension to start the reaction. Before starting light irradiation, in order to achieve the adsorption–desorption equilibrium of organic compounds on $LnFeO_3$ (Ln = La, Pr, or Gd), the suspension was magnetically stirred in the dark for a predetermined amount of time (e.g., 30 min for RhB and MO solution or 60 min for KP and TC solution). The suspension was then left in the presence of simulated visible light for 90 min. To determine the organic concentration, a small amount of sample was taken out from the suspension at a given period of time, centrifuged at 10,000 rpm, and then analyzed using a UV/Vis spectrophotometer. All tests were carried out under the same operation conditions, including illuminated area (24 cm^2) and power density (monitored by TES 132-Solar power meter).

3. Results and discussion

3.1 Material characterization

Fig. 1 shows that XRD patterns of $LnFeO_3$ (Ln = La, Pr, and Gd), which match well with the JCPDS files of $LaFeO_3$ (No. 37-1493) (Chandradass and Kim 2010), $PrFeO_3$ (No. 78-2424) (Qin *et al*. 2015) and $GdFeO_3$ (No. 47-0067) (Ding *et al*. 2010). It suggests that all samples are highly pure and crystalline with an orthorhombic structure. The crystallite sizes of $LaFeO_3$, $PrFeO_3$, and $GdFeO_3$ were calculated to be 28.0 nm, 19.6 nm, and 29.4 nm, respectively. Table 2 summarizes the cell volumes, lattice parameters, and corresponding tolerance factors for $LaFeO_3$, $PrFeO_3$, and $GdFeO_3$. The volumes and lattice parameters of resulting $LnFeO_3$ (Ln = La, Pr, and Gd) are in a good agreement with the reference (Berenov *et al*. 2008). The tolerance factor (t), defined as $t = (rA + rO)/2(rB + rO)$, where rA, rB, and rO are the individual ionic radii (Eitel *et al*. 2001), can be used as an indicator for the relative stability and distortion of $LnFeO_3$ crystal structures. Table 2 shows that the tolerance factors in this study decrease in an order of $LaFeO_3$ > $PrFeO_3$ > $GdFeO_3$. This is in line with the change of Ln^{3+} ionic radius in $LnFeO_3$ (La^{3+} (1.16) > Pr^{3+} (1.13) > Gd^{3+} (1.05)) (Li *et al*. 2006). Moreover, the degree of FeO_6 octahedron distortion in $LnFeO_3$ was found to decrease from La, Pr to Gd, according to the previous study (Berenov *et al*. 2008). The distortion of $LnFeO_3$ crystal structures would have a significant impact on the properties of $LnFeO_3$, including photocatalytic activity (Zhang *et al*. 2016).

Fig. 2 and Fig. 3 show the SEM and TEM images of $LnFeO_3$ (Ln = La, Pr, and Gd). All of the samples exhibit agglomeration of spherical particles, which are solid with no apparent pores in them. In particular, some smaller particles are seen to deposit on the $PrFeO_3$ and $GdFeO_3$ particle surfaces (Fig. 2a and b), which might be explained by the dissolution – recrystallization during hydrothermal reaction (Thirumalairajan *et al*. 2012a). Fig. 2d shows the

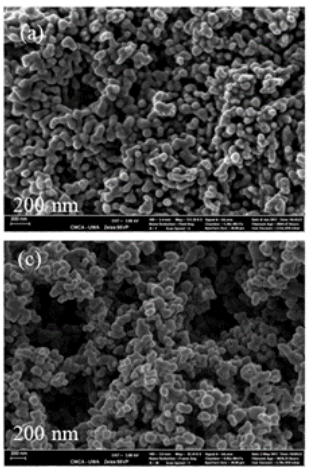

(d)

Samples	Compositions (at.%)		
	Ln (La, Pr, Ge)	Fe	O
$GdFeO_3$	20.52	24.29	56.42
$PrFeO_3$	20.92	20.21	58.88
$LaFeO_3$	20.52	19.48	60.00

Fig. 2 SEM images of (a) $GdFeO_3$, (b) $PrFeO_3$, and (c) $LaFeO_3$, and (d) their corresponding EDX data

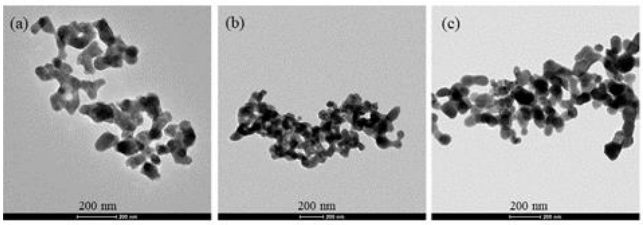

Fig. 3 TEM images of (a) $GdFeO_3$, (b) $PrFeO_3$, and (c) $LaFeO_3$

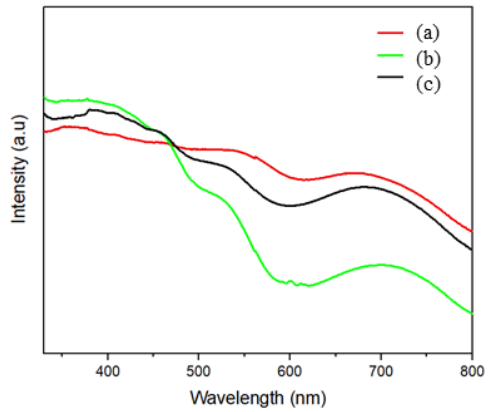

Fig. 4 UV-DRS absorption spectrum of (a) $GdFeO_3$, (b) $PrFeO_3$, and (c) $LaFeO_3$

Table 3 Structural properties of $GdFeO_3$, $PrFeO_3$ and $LaFeO_3$

Sample	S_{BET} (m^2/g)	Pore volume (cm^3/g)	Pore size (nm)
$GdFeO_3$	10.51	0.02	44.90
$PrFeO_3$	11.01	0.03	16.21
$LaFeO_3$	17.63	0.10	45.66

elemental compositions of $LnFeO_3$ (Ln = La, Pr, and Gd) by using EDX. It confirms the presence of Ln (Ln = Gd, Pr, or La), Fe, and O with the Ln/Fe/O molar ratio of 1/1/3, which is in agreement with the stoichiometric compositions of our as-prepared samples.

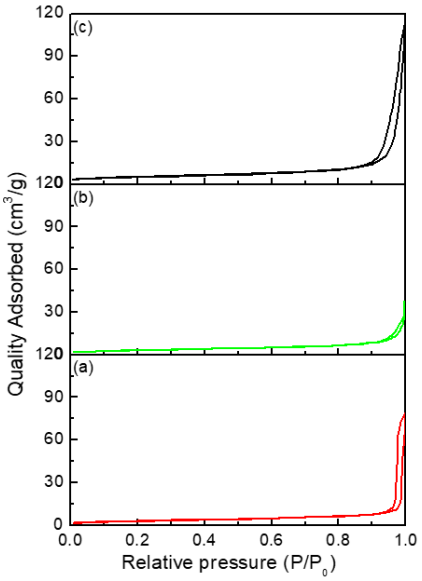

Fig. 5 Nitrogen adsorption-desorption isotherms of (a) $GdFeO_3$, (b) $PrFeO_3$ and (c) $LaFeO_3$

Table 4 Pseudo-first-order reaction rate constants for photo-Fenton degradation using $GdFeO_3$, $PrFeO_3$ and $LaFeO_3$

Catalyst	Organic pollutant	Kinetic rate constant (min^{-1})
$GdFeO_3$	KP	0.0066
$PrFeO_3$		0.0074
$LaFeO_3$		0.0136
$GdFeO_3$	TC	0.0231
$PrFeO_3$		0.0319
$LaFeO_3$		0.0486
$GdFeO_3$	MO	0.0026
$PrFeO_3$		0.0045
$LaFeO_3$		0.0052
$GdFeO_3$	RhB	0.0127
$PrFeO_3$		0.0164
$LaFeO_3$		0.0525

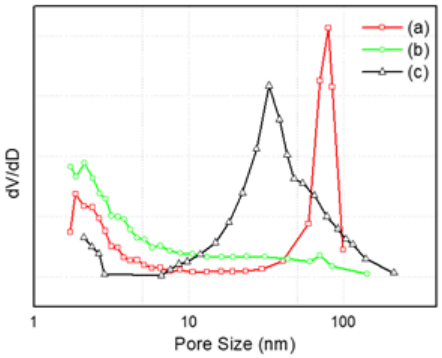

Fig. 6 BJH pore size distribution of (a) $GdFeO_3$, (b) $PrFeO_3$ and (c) $LaFeO_3$

The UV-vis absorption spectra (Fig. 4) of $LnFeO_3$ (Ln = La, Pr, and Gd) reveal that the absorption bands are in the visible region (400 nm – 800 nm), suggesting all materials

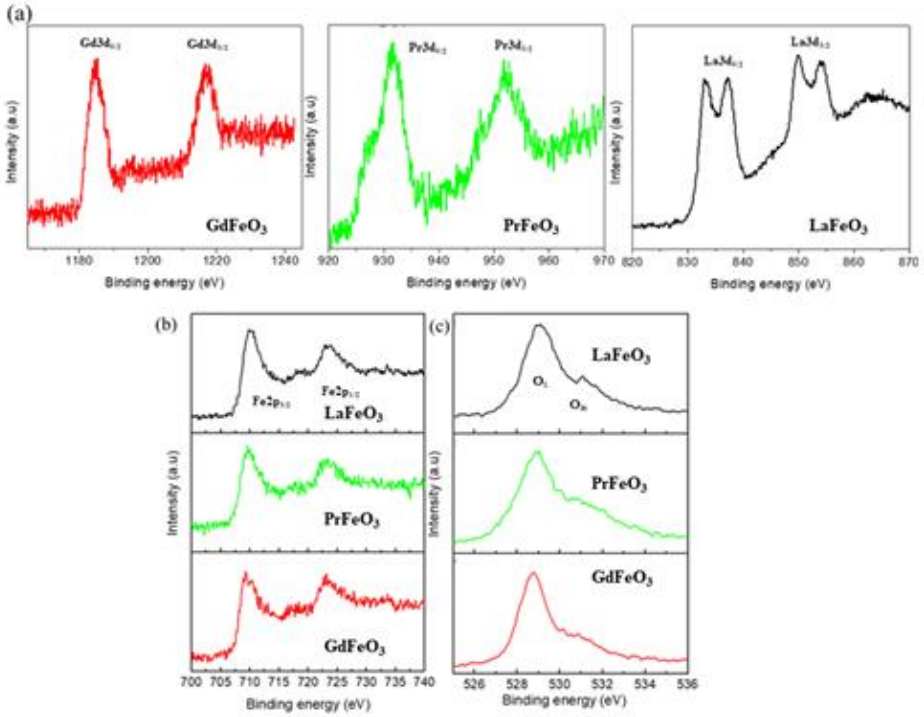

Fig. 7 XPS spectra of $GdFeO_3$, $PrFeO_3$ and $LaFeO_3$: (a) Ln 3d, (b) Fe 2p and (c) O 1s

could absorb visible light and exhibit visible-light-assisted photocatalytic activity. The values of band gap for $GdFeO_3$, $PrFeO_3$ and $LaFeO_3$ were calculated to be 2.6 eV, 2.4 eV and 2.3 eV, respectively. Especially, the sample of $LaFeO_3$ shows the narrow band gap energy, indicating its predominant absorptivity for visible light. The literature has revealed that the bonding in the corner-sharing FeO_6 octahedral network was the main factor affecting the band gap of $LnFeO_3$ (Mizoguchi *et al*. 2004). The Fe-O-Fe bond angles decrease as a result of the reduced ionic radii (Zhao *et al*. 2013), which leads to the expansion of Fe-centered octahedral network in the $LnFeO_3$ samples, following the order: $LaFeO_3$ > $PrFeO_3$ > $GdFeO_3$ (Table 2). This may decrease the antibonding Fe-O interaction and thus lower the energy of conduction band and band gap energy (Mizoguchi *et al*. 2004).

Fig. 5 shows the nitrogen adsorption–desorption isotherms of $GdFeO_3$, $PrFeO_3$, and $LaFeO_3$, while Table 3 summarizes their specific surface areas, pore volumes, and pore diameters. All samples herein show type IV isotherms with H3 hysteresis loops (Thirumalairajan *et al*. 2014). The hysteresis loops appear at the high relative pressure ranging from 0.9 to 1, which can be correlated to the interstitial holes formed between aggregated particles (Thirumalairajan *et al*. 2013). Fig. 6 demonstrates the BJH pore size distribution of three samples. Large peaks are at around 80 nm and 30 nm for $GdFeO_3$ and $LaFeO_3$. Interestingly, $PrFeO_3$ exhibits the distribution of much smaller pores. It is believed that large pores herein would greatly promote organic transport from solution to active sites on the catalyst. As is known, the photo-Fenton reaction usually occurs on the surface of a catalyst, the material with small crystallite size and large specific surface area would have enhanced photocatalytic activity (Li *et al*. 2007). The sample of $LaFeO_3$ possesses such favourable features.

Fig. 7 shows the XPS spectra for $GdFeO_3$, $PrFeO_3$ and $LaFeO_3$. In Fig. 7a, the binding energy of Gd $3d_{5/2}$ and Gd $3d_{3/2}$ is seen at 1185.4 eV and 1217.8 eV, respectively, suggesting the oxide form of the Gd^{3+} in the sample of $GdFeO_3$ (Söderlind *et al*. 2009). A doublet located at 931.7 eV and 951.7 eV corresponds to the core lines of Pr $3d_{5/2}$ and Pr $3d_{3/2}$ of Pr^{3+} in the sample of $PrFeO_3$ (Pandey *et al* 2005). For $LaFeO_3$, two strong peaks of La $3d_{5/2}$ and La $3d_{3/2}$ are located at 834.2 eV and 850.4 eV, which correspond to the core level spectra of La^{3+} ions in their oxide form (Thirumalairajan *et al*. 2012b). For all $LnFeO_3$, there is not much variation on the peak positions of Fe 2p (Fig. 7b), that two strong peaks of Fe $2p_{3/2}$ and Fe $2p_{1/2}$ are at 710.5 eV and 723.8 eV, assigned to the +3 oxidation state of Fe (Thirumalairajan *et al*. 2012b). The main O form in $LnFeO_3$ is O^{2-}, as indicated by the O 1s spectra corresponds to crystal lattice oxygen O_L (peaks situated at 529.0 eV) and hydroxyl oxygen O_H (peaks situated at 531.0 eV) (Parida *et al*. 2010). The XPS results herein agree with the above XRD and EDS results.

3.2 Photo-Fenton catalytic activity

The photo-Fenton catalytic activities of $LnFeO_3$ (Ln = La, Pr, and Gd) were examined for the removal of selected models of pharmaceuticals (KP and TC) and dyes (MO and RhB) under simulated visible light (λ > 400 nm) and in the presence of H_2O_2. Figs. 8(a)-(c), 11(a)-(c) present the corresponding results, as well as their comparison with the removal rates under the conditions by varying the use of visible light, H_2O_2, or/and catalyst. The pseudo-first-order reaction rate constants for photo-Fenton-induced degradation

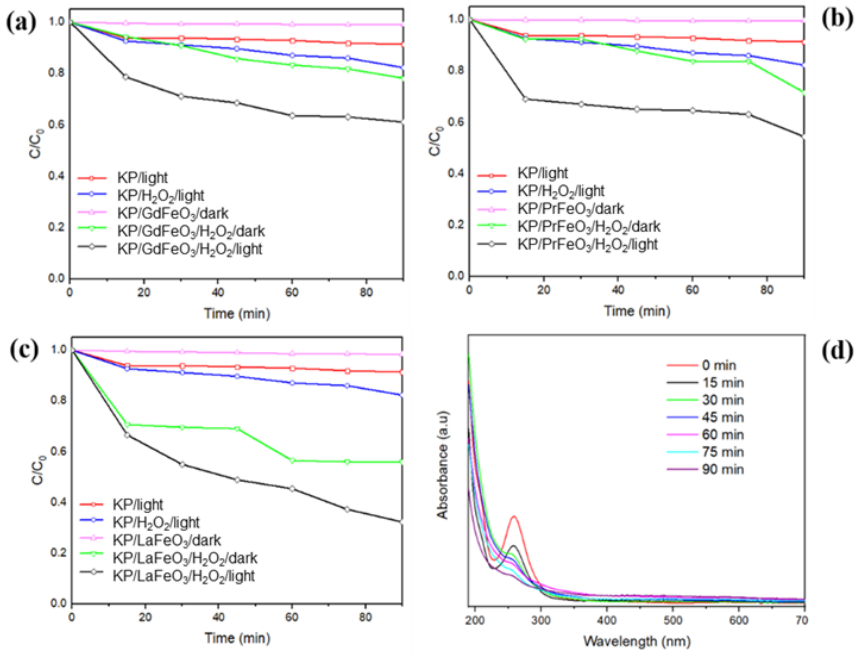

Fig. 8 KP removal in the photo-Fenton reaction using $GdFeO_3$ (a), $PrFeO_3$ (b), and $LaFeO_3$ (c) (catalyst dosage: 1 g/L, H_2O_2 concentration: 10 mM, KP concentration: 10 μM, pH: 5), as compared with those observed under different conditions by varying the use of visible light, H_2O_2, or/and catalyst, (d) KP temporal UV-Vis absorption spectra during the photo-Fenton reaction using $LaFeO_3$

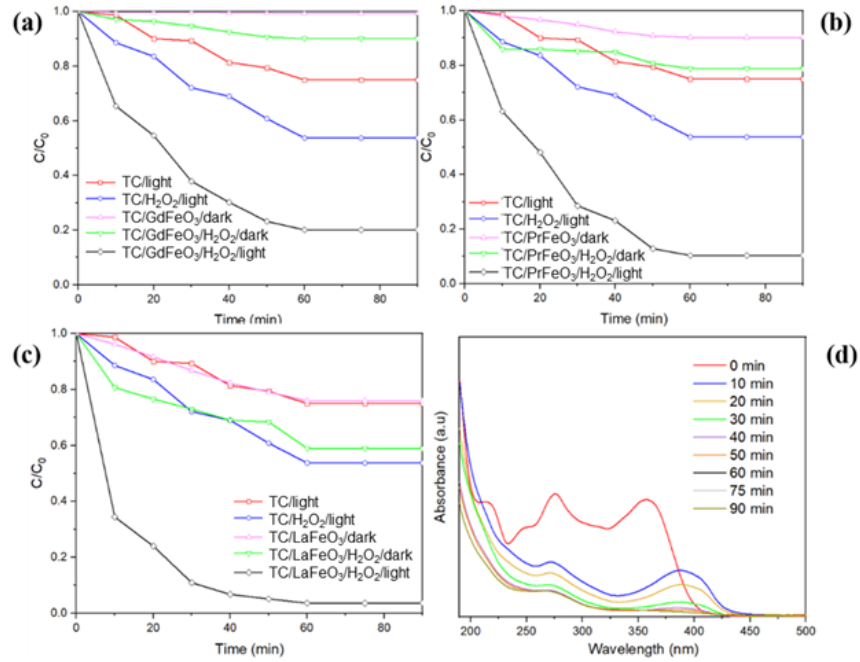

Fig. 9 TC removal in the photo-Fenton reaction using $GdFeO_3$ (a), $PrFeO_3$ (b), and $LaFeO_3$ (c) (catalyst dosage: 1 g/L, H_2O_2 concentration: 10 mM, TC concentration: 10 μM, pH: 5), as compared with those observed under different conditions by varying the use of visible light, H_2O_2, or/and catalyst, (d) TC temporal UV-Vis absorption spectra during the photo-Fenton reaction using $LaFeO_3$

of organics by using $LnFeO_3$ (Ln = La, Pr, and Gd) are summarized in Table 4. Figs. 8(d), 9(d), 10(d) and 11(d) show the temporal UV-Vis absorption spectra of KP, TC, MO, and RhB during the photo-Fenton reaction using $LaFeO_3$, respectively.

In Fig. 8, the light-assisted self-degradation of KP or its oxidation by visible light/H_2O_2 is limited (only 8.6% or 17.7%) in the absence of $LnFeO_3$ (Ln = La, Pr, and Gd). On the other side, in the dark, only around 2% KP adsorption onto $LnFeO_3$ is seen. Note that a significantly greater KP

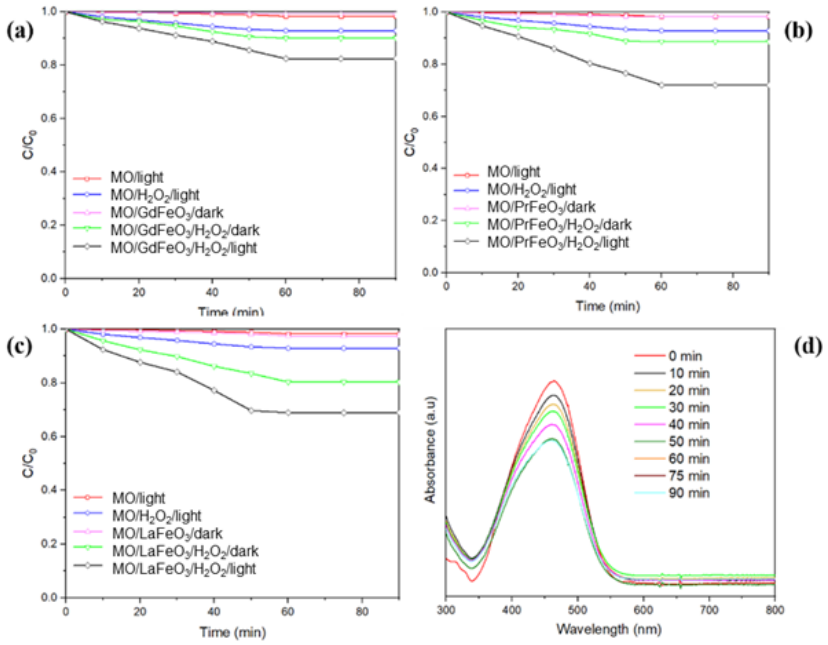

Fig. 10 MO removal in the photo-Fenton reaction using $GdFeO_3$ (a), $PrFeO_3$ (b), and $LaFeO_3$ (c) (catalyst dosage: 1 g/L, H_2O_2 concentration: 10 mM, MO concentration: 10 mg/L, pH: 5), as compared with those observed under different conditions by varying the use of visible light, H_2O_2, or/and catalyst, (d) MO temporal UV-Vis absorption spectra during the photo-Fenton reaction using $LaFeO_3$

removal is observed after 90-min Fenton reaction (in the dark/H_2O_2) using $GdFeO_3$ (21.8%), $PrFeO_3$ (28.3%) or $LaFeO_3$ (44%) (Fig. 8(a)-(c)). In the photo-Fenton process, the removal rate of KP with the use of $LaFeO_3$ reaches up to 67.6%, which is much greater than that induced using $PrFeO_3$ (45.5%) or $GdFeO_3$ (38.9%). The temporal UV-Vis absorption spectra of KP following the photo-Fenton reaction with the use of $LaFeO_3$ are shown in Fig. 8d. The major KP absorption peak at 260 nm steadily decreases, accompanied by a reduced absorption that slightly shifts towards the wavelength at 250 nm when the exposure to simulated light irradiation is extended from 0 min to 90 min. This suggests the breakdown of KP and then the production of byproducts (Canle *et al*, 2013, Djouadi *et al*. 2018).

On the other side, the utilization of light irradiation dramatically enhances the TC removal (Fig. 9) due to TC's nature of light sensitivity (Chen *et al*. 2008). In the absence of a catalyst, for instance, 25% of TC is removed by self-photolysis when being illuminated by visible light, whilst 46.3% of TC is reduced when both visible light and H_2O_2 are present. Less than 40% removal rate is achieved in the Fenton reaction using $LnFeO_3$ in the dark/H_2O_2. Interestingly, our experiment reveals that $LaFeO_3$ adsorbs 24% of TC in the dark when the adsorption–desorption equilibrium is reached, as compared with 1% or 10% by utilizing $GdFeO_3$ or $PrFeO_3$. The complexation between the La element and TC could be the reason to explain that (Vu *et al*. 2010). As is widely known, the heterogenous photo-Fenton reaction occurs at the active sites that are situated on the catalyst surfaces, a high adsorption capacity is one of the advantageous features for a catalyst facilitating access of organics and in turn increasing degradation efficiency. In the photo-Fenton reaction, the TC removal rate using $LaFeO_3$ (96.4%) is higher, in comparison to the utilization of $PrFeO_3$ (89.7%) or $GdFeO_3$ (79.9%). The self-photolysis ability of TC is also expected to more or less contribute to the superior TC removal % in the photo-Fenton reaction. The temporal UV-Vis absorption spectra of TC in the photo-Fenton reaction using $LaFeO_3$ (Fig. 9d) show two main absorption peaks at 275 nm and 360 nm, the absorption intensity of the peak at 360 nm decays much faster than that at 275 nm. According to the literature (Safari *et al*. 2015), such change might be explained by the stability of rings with N-groups in the structure of TC, which correspond to the absorbance at 275 nm, or the generation of intermediate products, which leads to the absorption at this wavelength. The significantly reduced absorption band at 360 nm, which is originated from aromatic rings, including the developed chromophores, indicates the fragmentation of phenolic groups attached to aromatic rings by the radicals produced in the photo-Fenton reaction. It is noted that the reduction of absorption band at 360 nm associated with the occurrence of new absorption at ~ 388 nm, which might be due to the formation of 4a,12a-anhydro-4-oxo-4-dedimethyl-aminotetracycline (Addamo *et al*. 2005, Safari *et al*. 2015, Zhu *et al*. 2013).

The catalytic performances of $LnFeO_3$ were also evaluated for the removal of anionic dye MO and cationic dye RhB. Our findings reveal that, in the absence of $LnFeO_3$, the chosen models of dyes (MO and RhB) show good stability when being exposed to simulated visible light and/or H_2O_2. Only < 8% of dye is removed from water. We also investigated the adsorption capability of $LnFeO_3$

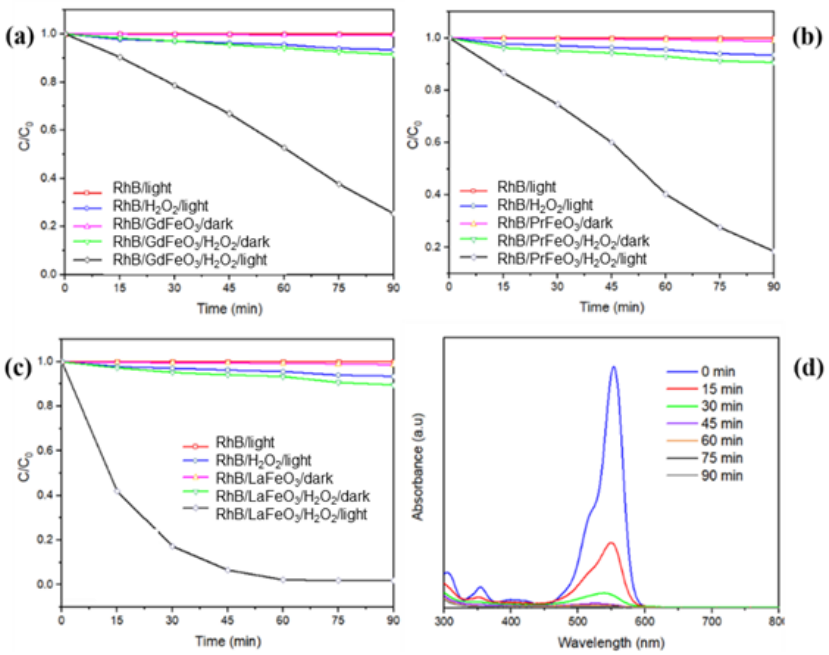

Fig. 11 RhB removal in the photo-Fenton reaction using $GdFeO_3$ (a), $PrFeO_3$ (b), and $LaFeO_3$ (c) (catalyst dosage: 1 g/L, H_2O_2 concentration: 10 mM, RhB concentration: 10 mg/L, pH: 5), as compared with those observed under different conditions by varying the use of visible light, H_2O_2, or/and catalyst, (d) RhB temporal UV-Vis absorption spectra during the photo-Fenton reaction using $LaFeO_3$

towards MO and RhB in the dark, however, < ~3% is seen suggesting insignificant attachment of organics onto the surfaces of catalysts. In Fig. 10, of three different $LnFeO_3$ samples, $LaFeO_3$ shows the highest photo-Fenton removal of MO (31.1%) in the presence of simulated visible light/H_2O_2, as compared with 19.7% MO removal *via* the Fenton reaction using $LaFeO_3$ (Fig. 10). On the other side, a smallest amount of MO, 17.6 or 9.9%, is removed by $GdFeO_3$ after the photo-Fenton or Fenton process. The removal of RhB induced by the Fenton reaction using $GdFeO_3$, $PrFeO_3$, and $LaFeO_3$ is only 8.5%, 9.3% and 10.4 %, respectively, in the dark. By contrast, the photo-Fenton reaction with the presence of $LnFeO_3$ results in more than 80% of RhB removal. Especially Fig. 11c shows that the nearly complete decolorization of RhB (98.2%) can be obtained within 90 min when using $LaFeO_3$.

It should be noted that the removal of MO (Fig. 10) *via* the photo-Fenton using $LnFeO_3$ is much lower as compared to that of RhB (Fig. 11), this might be attributed to the low photosensitized property and high chemical stability of MO (Shi *et al*. 2012). The time-dependent photo-Fenton degradation of MO and RhB as monitored by the main absorption bands (at 464 and 554 nm, respectively) over $LaFeO_3$ is presented in Figs. 10(d) and 11(d). In particular, the characteristic adsorption band of RhB at 554 nm rapidly decays within the first 60 min, implying that RhB is degraded under simulated visible light illumination following the de-ethylation process of RhB (Shi *et al*. 2014).

Table 5 lists the comparison of removal for the selected organics (MO, RhB and TC) with the use of our synthesized $LaFeO_3$ and other perovskites reported in the literature. It should be noted that so far, there has been no previous report on the removal of KP *via* photo-Fenton using our selected types of perovskites. In comparison with other perovskite photocatalysts (Li *et al*. 2014b, Zhou *et al*. 2016, Li *et al*. 2014a, Ju *et al*. 2011), our synthesized $LaFeO_3$ shows a promising photo-Fenton performance for RhB removal. The removal of MO or TC in our study is lower than those in some of previously published works (Tong *et al*. 2016, Xue *et al*. 2015), which might be explained by different types of perovskites selected and reaction conditions. In particular, we used a lower catalyst dosage, a smaller amount of hydrogen peroxide or/and the light source from a different company with lower power (Tong *et al*. 2016, Xue *et al*. 2015). Based on our observation and literature search (Khalil *et al*. 2022, Khairy *et al*. 2021), we believe our synthesized $LaFeO_3$ shows good application potential for photocatalytic conversion or/and removal of other organics, apart from our selected organic models herein. We also noted the optimization of $LaFeO_3$ synthesis may further boost its photocatalytic activity, including type of iron source, amount of citric acid and selection of heating temperature (Khalil *et al*. 2022, Phan *et al*. 2018a).

As shown in our study, the use of $LnFeO_3$ can lead to removal of selected pharmaceuticals (KP and TC) and dyes (MO and RhB) in the photo-Fenton reaction (with the use of simulated visible light/H_2O_2). This implies $LnFeO_3$ could work well as heterogeneous visible-light-active Fenton-like catalysts. Apparently as can be seen, that the photo-Fenton catalytic performances of $LnFeO_3$ differ, generally following the order of $GdFeO_3$ < $PrFeO_3$ < $LaFeO_3$ (Fig. 8-11), which is further supported by the kinetic rate constants shown in Table 4. The possible mechanisms governing the photo-Fenton catalytic degradation of organics can be explained *via* the synergism of two pathways, the hetero-

Table 5 Comparison of photo-Fenton catalytic activity between our $LaFeO_3$ and other perovskites in the literature for degradation of selected organics

Sample (Synthesis method)	Light source	Organics	Reaction conditions	Removal (%)	Ref.
$LaFeO_3$ (Hydrothermal method)	300 W Xe, $\lambda > 400$ nm	RhB, KP, TC, MO	TC or KP: dosage: 1.0 g/L, H_2O_2: 10 mM, organic: 10 μM, pH: 5, MO or RB: dosage: 1.0 g/L, H_2O_2: 10 mM, organic: 10 mg/L, pH: 5	67.7% (KP), 96.4% (TC), 31.1% (MO), 98.2% (RhB) after 1.5 h	This study
$BiFeO_3$ (Hydrothermal method)	500 W Xe, $\lambda > 420$ nm	MO	Dosage: 2.0 g/L, MO: 10 mg/L, H_2O_2: 80 mM	~97% after 3 h	(Tong *et al.* 2016)
$PrFeO_3$ and $YFeO_3$ (Sol-gel calcination)	500 W Xe, $\lambda > 400$ nm	RhB	Dosage: 1.0 g/L, RhB: 10^{-5} mol/L, H_2O_2: 1 mL of 3%	~25% ($YFeO_3$) and ~96% ($PrFeO_3$) after 2 h	(Li *et al.* 2014b)
$BiFeO_3$ (Hydrothermal method)	500 W halogen, 800 nm > λ > 420 nm	RhB	Dosage: 1.0 g/L, RhB: 10^{-5} mol/L, H_2O_2: 1 mL	~94% after 3 h	(Zhou *et al.* 2016)
$LaFeO_3$ and $SmFeO_3$ (Sol-gel calcination)	500 W Xe, $\lambda > 400$ nm	RhB	Dosage: 1.0 g/L, RhB: 10^{-5} mol/L, H_2O_2: 1 mL of 3%	89.6% ($SmFeO_3$) and over 97% ($LaFeO_3$) after 2 h	(Li *et al.* 2014a)
$EuFeO_3$ (Sol-gel calcination)	500 W Xe, $\lambda > 420$ nm	RhB	Dosage: 1.0 g/L, RhB: 5 mg/L, H_2O_2: 0.05 mL	71% after 3 h	(Ju *et al.* 2011)
$LaFeO_3$ (Sol-gel process and vacuum microwave calcination)	500 W Xe, $\lambda > 420$ nm	MO	MO: 10 mg/L, H_2O_2: 0.6 wt.%	91.9% after 4 h	(Shen *et al.* 2016)
$BiFeO_3$ (Hydrothermal method)	500 W Xe, $\lambda > 420$ nm	TC	Dosage: 0.5 g/L, TC: 10 mg/L, H_2O_2: 0.5 mM, pH: 5	100% after 40 min	(Xue *et al.* 2015)

generous Fenton-like reaction and semiconductor-induced photo-catalyzed oxidation (Li *et al.* 2014, Phan *et al.* 2018b). On the one side, the Fe atoms on the surfaces of $LnFeO_3$ can activate H_2O_2 to produce hydroxyl radicals in the Fenton reaction. On the other side, the catalyst of $LnFeO_3$ may generate electron–hole pairs under visible light illumination, in which the electrons are captured by H_2O_2 to produce active hydroxyl radicals. The generated hydroxyl radicals can directly oxidize and mineralize organics resulting in their removal from water. Based on the mechanisms, the observed variation in the photo-Fenton catalytic degradation using $LnFeO_3$ might be attributed to several reasons.

First of all, the variation on the species of rare earth Ln can result in the difference of $LnFeO_3$ crystal structures. In particular, the orthoferrite containing La, the ionic radius of which is greater than that of Pr or Gd, may exhibit a greater degree of structural distortion and then a higher photo-catalytic efficiency (Thirumalairajan *et al.* 2013). This is because structural distortions may serve as the hole–trapping centers, which could effectively reduce recombination rate between electrons and holes, and subsequently enhance the photo-Fenton removal of organics (Thirumalairajan *et al.* 2013, Chen and Umezawa 2014). A similar finding has also been reported by Ding and co-workers (Ding *et al.* 2010).

Secondly, it is believed that catalytic activity of $LnFeO_3$ is correlated to its band gap energy (Huang *et al.* 2010). The photo-Fenton degradation of organics over $LnFeO_3$ under visible light irradiation is affected by its light absorption ability. Smaller band gap of a catalyst is more beneficial for harvesting more photons to generate electrons and holes taking part in the photoreaction (Huang *et al.* 2010). Our calculation on the band gap energy of $LnFeO_3$ supports this.

Lastly, specific surface area and porous structure may impart an impact on the photo-Fenton catalytic degradation of organics. The degradation of organics occurs on the surface of a catalyst, at which there should be a good contact between the pollutant compound and the catalyst surface. Therefore, under visible light irradiation, a catalyst with higher specific surface area and greater porosity not only offers more active sites for photoreaction but also allows more surfaces reaching the light source, leading to the improved removal efficiency (Zhang *et al.* 2012). As shown in Table 3, $LaFeO_3$ possesses greatest surface area and pore volume, which are advantageous features for photo-Fenton reaction. We should also not neglect the improved adsorption caused by the correlation between organic (e.g., TC in this study) and catalyst ($LaFeO_3$) surfaces, that can be another factor contributing to the superior removal of pollutants in the photo-Fenton process.

4. Conclusions

We synthesized $LnFeO_3$ (Ln = La, Pr, and Gd) using the facile hydrothermal reaction and investigated their photo-Fenton-like catalytic activity for the removal of organic pollutants, including KP, TC, RhB, and MO, under simulated visible light irradiation. The variation of Ln-site atoms in $LnFeO_3$ not only caused a distortion of crystal structures but also had an impact on the band gap. The organic removal efficiency using $LnFeO_3$ was seen with an improvement in the following order of $LaFeO_3$ > $PrFeO_3$ > $GdFeO_3$. This may be explained by the structural distortion, band gap and specific surface area.

Acknowledgment

This research was funded by Vietnam National Foundation for Science and Technology Development (NAFOSTED) under grant number 104.05-2020.06.

The authors acknowledge the support received from Murdoch SEIT Small Grant Scheme (2016). T. Phan's PhD study was supported by Australia Awards Scholarship. The authors acknowledge the facilities, and the scientific and technical assistance of the Australian Microscopy & Microanalysis Research Facility at the Centre for Microscopy, Characterisation & Analysis, The University of Western Australia, a facility funded by the University, State and Commonwealth Governments. The authors thank Ms Caitlin Sweeney for band gap measurement and analysis.

References

Addamo, M., Augugliaro, V., Di Paola, A.V. Loddo, E.G.L. and Palmisano, L. (2005), "Removal of drugs in aqueous systems by photoassisted degradation", *J. Appl. Electrochem.*, **35**(7), 765-774. https://doi.org/10.1007/s10800-005-1630-y

Ahmad, M., Ahmed, E., Hong, Z.L., Ahmed, W., Elhissi, A. and Khalid, N.R. (2014), "Photocatalytic, sonocatalytic and sono-photocatalytic degradation of Rhodamine B using ZnO/CNTs composites photocatalysts", *Ultrasonics Sonochem.*, **21**(2), 761-773. https://doi.org/10.1016/j.ultsonch.2013.08.014

Aono, H., Sato, M., Traversa, E., Sakamoto, M. and Sadaoka, Y. (2001), "Design of ceramic materials for chemical sensors: effect of $SmFeO_3$ processing on surface and electrical properties", *J. Am. Ceram. Soc.*, **84**(2), 341-47. https://doi.org/10.1111/j.1151-2916.2001.tb00660.x

Bansal, P., Verma, A. and Talwar, S.J.C.E.J. (2018), "Detoxification of real pharmaceutical wastewater by integrating photocatalysis and photo-Fenton in fixed-mode", *Chem. Eng. J.*, 349, 838-848. https://doi.org/10.1016/j.cej.2018.05.140

Bafana, A., Devi, S.S. and Chakrabarti, T.J.E.R. (2011), "Azo dyes: Past, present and the future", *Environ. Rev.*, **19**, 350-371. https://doi.org/10.1139/a11-018

Bellakki, M.B., Kelly, B.J. and Manivannan, V. (2010), "Synthesis, characterization, and property studies of (La, Ag) FeO_3 ($0.0 \leq x \leq 0.3$) perovskites", *J. Alloys Compd.*, **489**(1), 64-71. https://doi.org/10.1016/j.jallcom.2009.08.059

Berenov, A., Angeles, E., Rossiny, J., Raj, E., Kilner, J. and Atkinson, A. (2008), "Structure and transport in rare-earth ferrates", *Solid State Ionics*, **179**(21), 1090-1093. https://doi.org/10.1016/j.ssi.2008.01.025

Canle López, M., Vilarino, S., Fernandez, M.I., Faria, J., Canle L., M. and Santaballa, J.A. (2013), "Mechanism of aqueous degradation of ketoprofen by heterogeneous photocatalysis", *Appl. Catal. B Environ.*, 142-143, 633-646. https://doi.org/10.1016/j.apcatb.2013.05.018

Chandradass, J. and Kim, K.H. (2010), "Nano-$LaFeO_3$ powder preparation by calcining an emulsion precursor", *Mater. Chem. Phys.*, **122**(2–3), 329-332. https://doi.org/10.1016/j.matchemphys.2010.03.039

Chequer, F.M.D., de Oliveira, G.A.R., Ferraz, E.R.A., Cardoso, J.C., Zanoni, M.V.B. and de Oliveira, D.P. (2013) *Textile Dyes: Dyeing Process and Environmental Impact*, in *Eco-Friendly Textile Dyeing and Finishing*, M. Günay, Editor. https://doi.org/10.5772/53659

Chen, H. and N. Umezawa, (2014), "Hole localization, migration, and the formation of peroxide anion in perovskite $SrTiO_3$", *Phys. Rev. B*, **90**(3), 035202. https://doi.org/10.1103/PhysRevB.90.035202

Chen, Q., Wu, P., Li, Y., Zhu, N. and Dang Z. (2009), "Heterogeneous photo-Fenton photodegradation of reactive brilliant orange X-GN over iron-pillared montmorillonite under visible irradiation", *J. Hazard. Mater.*, **168**(2), 901-908. https://doi.org/10.1016/j.jhazmat.2009.02.107

Chen, Y., Hu, C., Qu, J. and Yang, M. (2008), "Photodegradation of tetracycline and formation of reactive oxygen species in aqueous tetracycline solution under simulated sunlight irradiation", *J. Photochem. Photobiol. A Chem.*, **197**(1), 81-87. https://doi.org/10.1016/j.jphotochem.2007.12.007

Corcoran, J., Winter, M.J. and Tyler, C.R. (2010), "Pharmaceuticals in the aquatic environment: A critical review of the evidence for health effects in fish", *Critic. Rev. Toxicol.*, **40**(4), 287-304. https://doi.org/10.3109/10408440903373590

Deepeka, Kaur, P., Jyoti, Bansal, S. and Singhal S. (2022), "In-situ functionalized biomass derived graphite-supported $BiFeO_3$ for eradication of pollutants", *Adv. Nano Res.*, **13**(6) 527-543. https://doi.org/10.12989/anr.2022.13.6.527

Djouadi, L., Khalaf, H., Boukhatem, H., Boutoumi, H., Kezzime, A., Santaballa, J.A. and Canle, M. (2018), "Degradation of aqueous ketoprofen by heterogeneous photocatalysis using Bi_2S_3/TiO_2–Montmorillonite nanocomposites under simulated solar irradiation", *Appl. Clay Sci.*, **166**, 27-37. https://doi.org/10.1016/j.clay.2018.09.008

Ding, J., Lu, X., Shu, H., Xie, J. and Zhang, H. (2010), "Microwave-assisted synthesis of perovskite $ReFeO_3$ (Re: La, Sm, Eu, Gd) photocatalyst", *Mater. Sci. Eng. B*, **171**(1), 31-34. https://doi.org/10.1016/j.mseb.2010.03.050

Eitel, R.E., Randall, C.A., Shrout, T.R., Rehrig, P.W., Hackenberger, W. and Park S.-E. (2001), "New high temperature morphotropic phase boundary piezoelectrics based on Bi $(Me)O_3$–$PbTiO_3$ ceramics", *Japan. J. Appl. Phys.*, **40**(10R), 5999. https://doi.org/10.1143/JJAP.40.5999

Feng, J., Hu, X., Yue, P. L., Zhu, H. Y. and Lu, G. Q. (2003), "Discoloration and mineralization of Reactive Red HE-3B by heterogeneous photo-Fenton reaction", *Water Res.*, **37**(15), 3776-3784. https://doi.org/10.1016/S0043-1354(03)00268-9

Huang, Y., Wei, Y., Cheng, S., Fan, L., Li, Y., Lin, J. and Wu, J. (2010), "Photocatalytic property of nitrogen-doped layered perovskite $K_2La_2Ti_3O_{10}$", *Solar Energy Mater. Solar Cell.*, **94**(5), 761-766. https://doi.org/10.1016/j.solmat.2009.12.020

Ju, L., Chen, Z., Fang, L., Dong, W., Zheng, F. and Shen, M. (2011), "Sol–gel synthesis and photo-Fenton-like catalytic activity of $EuFeO_3$ nanoparticles", *J. Am. Ceram. Soc.*, **94**(10), 3418-3424. https://doi.org/10.1111/j.1551-2916.2011.04522.x

Khalil, K.M.S., Mahmoud, A.H. and Khairy, M. (2022). "Formation and textural characterization of size-controlled $LaFeO_3$ perovskite nanoparticles for efficient photocatalytic degradation of organic pollutants", *Adv. Powder Technol.*, **33**, 103429. https://doi.org/10.1016/j.apt.2022.103429

Khairy, M., Mahmoud, A.H. and Khalil, K.M.S. (2021). "Synthesis of highly crystalline $LaFeO_3$ nanospheres for phenoxazinone synthase mimicking activity", *RSC Adv.*, **11**, 17746-17754. https://doi.org/10.1039/D1RA02295D

Lee, H, Park, S.H., Park Y.K., Kim B.H., Kim S.J. and Jung S.C. (2013), "Rapid destruction of the rhodamine B using TiO_2 photocatalyst in the liquid phase plasma", *Chem. Centr. J.*, **7**(1), 156. https://doi.org/10.1186/1752-153X-7-156

Li, L. and Wang, X. (2016), "Self-propagating combustion synthesis and synergistic photocatalytic activity of $GdFeO_3$ nanoparticles", *J. Sol-Gel Sci. Technol.*, **79**(1), 107-113. https://doi.org/10.1007/s10971-016-4017-0

Li, L., Wang, X. and Zhang, Y. (2014a), "Enhanced visible light-responsive photocatalytic activity of $LnFeO_3$ (Ln = La, Sm) nanoparticles by synergistic catalysis", *Mater. Res. Bull.*, **50**, 18-22. https://doi.org/10.1016/j.materresbull.2013.10.027

Li, L., Zhang, M., Tian, P., Gu, W. and Wang, X. (2014b), "Synergistic photocatalytic activity of $LnFeO_3$ (Ln=Pr, Y) perovskites under visible-light illumination", *Ceram. Int.*, **40**(9), 13813-13817. https://doi.org/10.1016/j.ceramint.2014.05.097

Li, S., Jing, L., Fu, W., Yang, L., Xin, B. and Fu, H. (2007), "Photoinduced charge property of nanosized perovskite-type $LaFeO_3$ and its relationships with photocatalytic activity under visible irradiation", *Mater. Res. Bull.*, **42**(2), 203-212. https://doi.org/10.1016/j.materresbull.2006.06.010

Li, Z., Xue, H., Wang, X. and Fu, X. (2006), "Characterizations and photocatalytic activity of nanocrystalline $La_{1.5}Ln_{0.5}Ti_2O_7$ (Ln=Pr, Gd, Er) solid solutions prepared via a polymeric complex method", *J. Mol. Catal. A Chem.*, **260**(1), 56-61. https://doi.org/10.1016/j.molcata.2006.06.056

Martínez, C., Vilariño, S., Fernández, M.I., Faria, J., Canle L., M. and Santaballa, J.A. (2013), "Mechanism of degradation of ketoprofen by heterogeneous photocatalysis in aqueous solution", *Appl. Catal. B Environ.*, **142**, 633-646. https://doi.org/10.1016/j.apcatb.2013.05.018

Martínez-Huitle, C.A. and Brillas, E. (2009), "Decontamination of wastewaters containing synthetic organic dyes by electro-chemical methods: a general review", *Appl. Catal. B Environ.*, **87**(3), 105-145. https://doi.org/10.1016/j.apcatb.2008.09.017

Mizoguchi, H., Eng, H.W. and Woodward, P.M. (2004), "Probing the electronic structures of ternary perovskite and pyrochlore oxides containing Sn^{4+} or Sb^{5+}", *Inorgan. Chem.*, **43**(5), 1667-1680. https://doi.org/10.1021/ic034551c

Niaei H.A. and Rostamizadeh M. (2020), "Adsorption and electro-Fenton processes over FeZSM-5 nanozeolite for tetracycline removal from wastewater", *Adv. Nano Res.*, **9**(3), 173-181. https://doi.org/10.12989/anr.2020.9.3.173

Niu, X., Li, H. and Liu, G. (2005), "Preparation, characterization and photocatalytic properties of $REFeO_3$ (RE=Sm, Eu, Gd)", *J. Mol. Catal. A Chem.*, **232**(1), 89-93. https://doi.org/10.1016/j.molcata.2005.01.022

Oturan, M.A. and Aaron, J.J. (2014), "Advanced oxidation processes in water/wastewater treatment: Principles and applications. A review", *Critic. Rev. Environ. Sci. Technol.*, **44**(23), 2577-2641. https://doi.org/10.1080/10643389.2013.829765

Pandey, S.K., Bindu, R., Bhatt, P., Chaudhari, S.M. and Pimpale, A.V. (2005), "Synthesis and investigation of structural and electronic properties of $Pr_{1-x}Ca_xFeO_3$ ($0 \leqslant x \leqslant 0.2$) compounds", *Physica B Condens. Matter.*, **365**(1), 47-54. https://doi.org/10.1016/j.physb.2005.04.036

Parida, K.M., Reddy, K.H., Martha, S. Das D.P. and Biswal, N. (2010), "Fabrication of nanocrystalline $LaFeO_3$: An efficient sol–gel auto-combustion assisted visible light responsive photocatalyst for water decomposition", *Int. J. Hydrogen Energy*, **35**(22), 12161-12168. https://doi.org/10.1016/j.ijhydene.2010.08.029

Phan, T.T.N., Nikoloski, A.N., Bahri P.A. and Li, D. (2018a), "Optimizing photocatalytic performance of hydrothermally synthesized $LaFeO_3$ by tuning material properties and operating conditions", *J. Environ. Chem. Eng.*, **6**(1), 1209-1218. https://doi.org/10.1016/j.jece.2018.01.033

Phan, T.T.N., Nikoloski, A.N., Bahri P.A. and Li, D. (2018b), "Adsorption and photo-Fenton catalytic degradation of organic dyes over crystalline $LaFeO_3$-doped porous silica", *RSC Adv.*, **8**(63), 36181-36190. https://doi.org/10.1039/C8RA07073C

Phan, T.T.N., Nikoloski, A.N., Bahri P.A. and Li, D. (2018c), "Heterogeneous photo-Fenton degradation of organics using highly efficient Cu-doped $LaFeO_3$ under visible light", *J. Ind. Eng. Chem.*, **61**, 53-64. https://doi.org/10.1016/j.jiec.2017.11.046

Phan, T.T.N., Dinh, T.T.M., Nguyen, M.D., Li, D., Phan, C.N., Pham, T.K., Nguyen, C.T. and Pham, T.H. (2022), "Hierarchically structured $LaFeO_3$ with hollow core and porous shell as efficient sensing material for ethanol detection", *Sensors Actuat. B Chem.*, **354**, 131195. https://doi.org/10.1016/j.snb.2021.131195

Qin, C., Li, Z., Chen, G., Zhao, Y., Lin, T. (2015), "Fabrication and visible-light photocatalytic behavior of perovskite praseodymium ferrite porous nanotubes", *J. Power Sourc.*, **285**, 178-184. https://doi.org/10.1016/j.jpowsour.2015.03.096

Qiu, L., Ichikawa, T., Hirano, A., Imanishi, N., Takeda, Y. (2003), "$Ln_{1-x}Sr_xCo_{1-y}Fe_yO_{3-\delta}$ (Ln= Pr, Nd, Gd, x= 0.2, 0.3) for the electrodes of solid oxide fuel cells", *Solid State Ionics*, **158**(1), 55-65. https://doi.org/10.1016/S0167-2738(02)00757-9

Rodríguez-Gil, J.L., Catalá, M., Alonso, S.G., Maroto, R.R., Valcárcel, Y., Segura, Y., Molina, R., Melero, J.A., Martínez, F. (2010), "Heterogeneous photo-Fenton treatment for the reduction of pharmaceutical contamination in Madrid rivers and ecotoxicological evaluation by a miniaturized fern spores bioassay", *Chemosphere*, **80**(4), 381-388. https://doi.org/10.1016/j.chemosphere.2010.04.045

Söderlind, F., Selegard, L., Nordblad, P., Uvdal, K. and Kall, P.O. (2009), "Sol–gel synthesis and characterization of polycrystalline $GdFeO_3$ and $Gd_3Fe_5O_{12}$ thin films", *J. Sol-Gel Sci. Technol.*, **49**(2), 253-259. https://doi.org/10.1007/s10971-008-1859-0

Safari, G.H., Mahvi, A. H., Yaghmaeian, K., Nabizadeh, R. and Alimohammadi, M. (2015), "Optimization of sonochemical degradation of tetracycline in aqueous solution using sono-activated persulfate process", *J. Environ. Health Sci. Eng.*, **13**, 76-76. https://doi.org/10.1186/s40201-015-0234-7

Shah, A.H. and Rather M.A. (2021), "Pharmaceutical residues: new emerging contaminants and their mitigation by nano-photocatalysis", *Adv. Nano Res.*, **10**(4), 397-414. https://doi.org/10.12989/anr.2021.10.4.397

Shen, H., Xue, T., Wang, Y., Cao, G., Lu, Y. and Fang, G. (2016). "Photocatalytic property of perovskite $LaFeO_3$ synthesized by sol-gel process and vacuum microwave calcination", *Mater. Res. Bull.*, **84**, 15-24. https://doi.org/10.1016/j.materresbull.2016.07.024

Soon, A.N. and Hameed, B.H. (2011), "Heterogeneous catalytic treatment of synthetic dyes in aqueous media using Fenton and photo-assisted Fenton process", *Desalination*, **269**(1), 1-16. https://doi.org/10.1016/j.desal.2010.11.002

Shi, J.W., Yan, X., Cui, H.J., Zong, X., Fu, M.L., Chen, S., Wang, L. (2012), "Low-temperature synthesis of CdS/TiO_2 composite photocatalysts: Influence of synthetic procedure on photo-catalytic activity under visible light", *J. Mol. Catal. A Chem.*, **356**, 53-60. https://doi.org/10.1016/j.molcata.2012.01.001

Shi, J., Ai, Z. and Zhang, L. (2014), "$Fe@Fe_2O_3$ core-shell nanowires enhanced Fenton oxidation by accelerating the Fe(III)/Fe(II) cycles", *Water Res.*, **59**, 145-153. https://doi.org/10.1016/j.watres.2014.04.015

Thakur, P., Chahar, D. and Thakur, A. (2022), "Visible light assisted photocatalytic degradation of methylene blue dye using Ni doped Co-Zn nanoferrites", *Adv. Nano Res.*, **12**(4), 415-426. https://doi.org/10.12989/anr.2022.12.4.415

Thirumalairajan, S., Girjia, K., Ganesh I., Managalaraj, D., Viswanathan C., Balamurugan A. and Ponpandian N. (2012a), "Controlled synthesis of perovskite $LaFeO_3$ microsphere composed of nanoparticles via self-assembly process and their associated photocatalytic activity", *Chem. Eng. J.*, **209**, 420-428. https://doi.org/10.1016/j.cej.2012.08.012

Thirumalairajan, S., Girjia, K., Ganesh V., Managalaraj, D., Viswanathan C. and Ponpandian N. (2012b), "Novel synthesis of $LaFeO_3$ nanostructure dendrites: A systematic investigation of growth mechanism, properties, and biosensing for highly selective determination of neurotransmitter compounds", *Cryst. Growth Des.*, **13**(1), 291-302. https://doi.org/10.1021/cg3014305

Thirumalairajan, S., Girjia, K., Mastelaro V.R., Ganesh V. and Ponpandian N. (2014), "Detection of the neurotransmitter dopamine by a glassy carbon electrode modified with self-assembled perovskite $LaFeO_3$ microspheres made up of nanospheres", *RSC Adv*., **4**(49), 25957-25962. https://doi.org/10.1039/C4RA03467H

Thirumalairajan, S., Girjia, K., Hebalkar, N.Y., Managalaraj, D., Viswanathan, C. and Ponpandian N. (2013), "Shape evolution of perovskite $LaFeO_3$ nanostructures: a systematic investigation of growth mechanism, properties and morphology dependent photocatalytic activities", *RSC Adv*., **3**(20), 7549-7561. https://doi.org/10.1039/C3RA00006K

Tong, T., Zhang, H., Chen, J., Jin, D. and Cheng J. (2016), "The photocatalysis of $BiFeO_3$ disks under visible light irradiation", *Catal. Commun*., **87**, 23-26. https://doi.org/10.1016/j.catcom.2016.08.030

Vu, B.K., Snisarenko, O., Lee H. S., Shin E. W. (2010), "Adsorption of tetracycline on La-impregnated MCM-41 materials", *Environ. Technol*., **31**(3), 233-241. https://doi.org/10.1080/09593330903453210

Xue, Z., Wang, T., Chen, B., Malkoske, T., Yu, S., Tang, Y. (2015), "Degradation of tetracycline with $BiFeO_3$ prepared by a simple hydrothermal method", *Materials*, **8**(9), 6360-6378. http:/doi.org/10.3390/ma8095310

Yeşilova, E., Osman, B., Kara, A., Ozer, E.T. (2018), "Molecularly imprinted particle embedded composite cryogel for selective tetracycline adsorption", *Sep. Purif. Technol*., **200**, 155-163. https://doi.org/10.1016/j.seppur.2018.02.002

Zhang, G., Liu, G., Wang, L. and Irvine, J.T.S. (2016), "Inorganic perovskite photocatalysts for solar energy utilization", *Chem. Soc. Rev.*, **45**(21), 5951-5984. https://doi.org/10.1039/C5CS00769K

Zhang, P., Shao, C., Zhang, M., Guo, Z., Mu, J., Zhang, Z., Zhang, X. and Liu, Y. (2012), "Bi_2MoO_6 ultrathin nanosheets on $ZnTiO_3$ nanofibers: A 3D open hierarchical heterostructures synergistic system with enhanced visible-light-driven photo-catalytic activity", *J. Hazard. Mater*., **217**, 422-428. https://doi.org/10.1016/j.jhazmat.2012.03.046

Zhao, H.J., Ren, W., Yang, Y., Chen, X. M., Bellaiche, L. (2013), "Effect of chemical and hydrostatic pressures on structural and magnetic properties of rare-earth orthoferrites: a first-principles study", *J. Phys. Condens. Matter*., **25**(46), 466002. https://doi.org/10.1088/0953-8984/25/46/466002

Zhou, M., Li, W., Du, Y., Kong, D., Wang, Z., Meng, Sun, X., Yan, T., Kong D. and You, J. (2016), "Hydrothermal synthesis of bismuth ferrite Fenton-like catalysts and their properties", *J. Nanopart. Res.*, **18**(11), 346. https://doi.org/10.1007/s11051-016-3665-x

Zhu, J., Li, H., Zhong, L., Xiao, P., Xu X., Yang, X., Zhao, Z. and Li, J. (2014), "Perovskite oxides: preparation, characterizations, and applications in heterogeneous catalysis", *ACS Catal*., **4**(9), 2917-2940. https://doi.org/10.1021/cs500606g

Zhu, X.D., Wang, Y.J., Sun, R.J. and Zhou, D.M. (2013), "Photocatalytic degradation of tetracycline in aqueous solution by nanosized TiO_2", *Chemosphere*, **92**(8), 925-932. https://doi.org/10.1016/j.chemosphere.2013.02.066